Stability Analysis of Oscillations in SVCs

Zhengyu Wang, Lingling Fan, Zhixin Miao
Department of Electrical Engineering
University of South Florida
Tampa, FL 33620, USA
email: {zhengyuwang, zmiao, linglingfan}@usf.edu

***Abstract*—Static var compensators (SVCs) have been popularly installed to provide voltage support. It is well known by the grid industry that large voltage control gain may lead to instability, especially in weak grids when the grid impedance becomes large. Analytical models have been developed for eigenvalue analysis. This approach requires tremendous modeling efforts besides the electromagnetic transient (EMT) simulation test bed setup. In this paper, we use measurements obtained from an EMT simulation test bed to extract the linear model that reflects the relationship between SVC's susceptance command and the point of connection voltage magnitude. Analysis based on the open-loop system consisting of the voltage controller and the learned linear model shows that oscillations are mainly due to time delay introduced by thyristor switching devices and digital control. Increasing voltage control and reducing the system strength push the oscillation mode towards the right half plane (RHP). The measurement-based stability analysis approach provides a simple, straightforward, yet powerful tool to characterize stability issues.**

***Index Terms*—SVC, Oscillations, Stability Analysis.**

I. Introduction

Static VAR Compensator (SVC), has been widely installed as a type of flexible alternating current transmission systems (FACTs) for voltage support, power factor correction, and system stabilizing [1]. For example, in 1980s, American Electric Power (AEP) placed two 125-MVAr SVCs in Kentucky to reinforce a 138-kV transmission system [2], [3]. Maine Electric Power Company installed a -125/+425MVAR SVC in the 345-kV system at Chester Maine to support 700 MW importing into the New England network [4].

Oscillation phenomena associated with SVC have also been reported, with [5] or without series compensation [6] in the network. For oscillations in SVCs in weak grids, research carried out in 1990s pointed out that the most critical factors are the compensation level, the voltage control parameters, the grid strength, and the time delay due to controller and thyristor firing units [6].

Most recently, the Central Tibet Interconnection Project (CTAIP) in China observed oscillations in EMT simulations of SVCs installed in a long-chain network from center Tibet to Chengdu, Sichuan power grid [7]. Additionally, oscillations appeared in the study of Zangzhong Interconnection in China due to two sets of 60-MVAr SVCs in weak grid [8].

The stability analysis conducted from the above research requires analytical models. Analytical model building, e.g., [9], requires additional efforts for not only modeling but also validation and benchmarking with the EMT test bed. In this paper, we completely rely on a EMT test bed with full details of SVC control and thyristor firing for both time-domain simulation and linear system analysis. Our paper presents measurement-based stability analysis to investigate why large voltage gain and weak grid strength may lead to instability.

The rest of the paper is organized as follows. Section II introduces the EMT test bed and the time-domain results. Section III presents the time-domain measurement data collection and linear model extraction. Section IV presents stability analysis using the linear models. The conclusion is stated in Section V.

II. EMT Modeling-based Analysis

A. Study System and Phenomenon

To study an SVC in the weak grid, an EMT testbed shown in Fig. 1 is implemented via MATLAB/Simulink with SimPowerSystems Toolbox. This test bed is adapted from the demo SVC detailed model in SimPowerSystem by Pierre Giroux and Gibert Sybille (Hydro-Quebec) [10]. A 200-MW resistive load is connected to a 735-kV infinite bus through a long chain network. The simulation sampling time is 50 μs.

The 16-kV, -100/300-MVAr SVC structure includes one six-pulse thyristor-controlled reactor (TCR) and three thyristor-controlled capacitors in Δ-connected topology. The SVC is connected to the load bus through an $\mathrm{Y_g}-\Delta$ connected 735-kV/16-kV transformer. The SVC is controlled by firing pulses generated according to the voltage regulator shown in Fig. 2.

The model is modified to serve the research purpose. Original transmission line short-circuit power is 6000 MVA, and it is lowered to 2000 MVA to represent a weaker grid connection. The droop gain is set to zero so that the controller only includes the voltage regulator. Default control parameters are $k_p = 0$ and $k_i = 800$, and they are changed to present the oscillation phenomenon. All the modeling parameters are listed in Table. I.

The default line impedance, X_{g}, is 0.05 p.u. Fig. 3 presents the simulation results after a step increase of 0.03 p.u. on the voltage reference. The voltage control' gains are increased by 4.5 fold from its base values: $k_p = 45$ and $k_i = 900$. The spectrum plot shown in Fig. 4 indicates that only 36-Hz sub-synchronous oscillation appears in the measurements of voltage magnitude and reactive power output by SVC, and both 24-Hz and 96-Hz oscillations exist in the ac current flows from the SVC.

978-1-6654-9921-7/22/$31.00 ©2022 IEEE

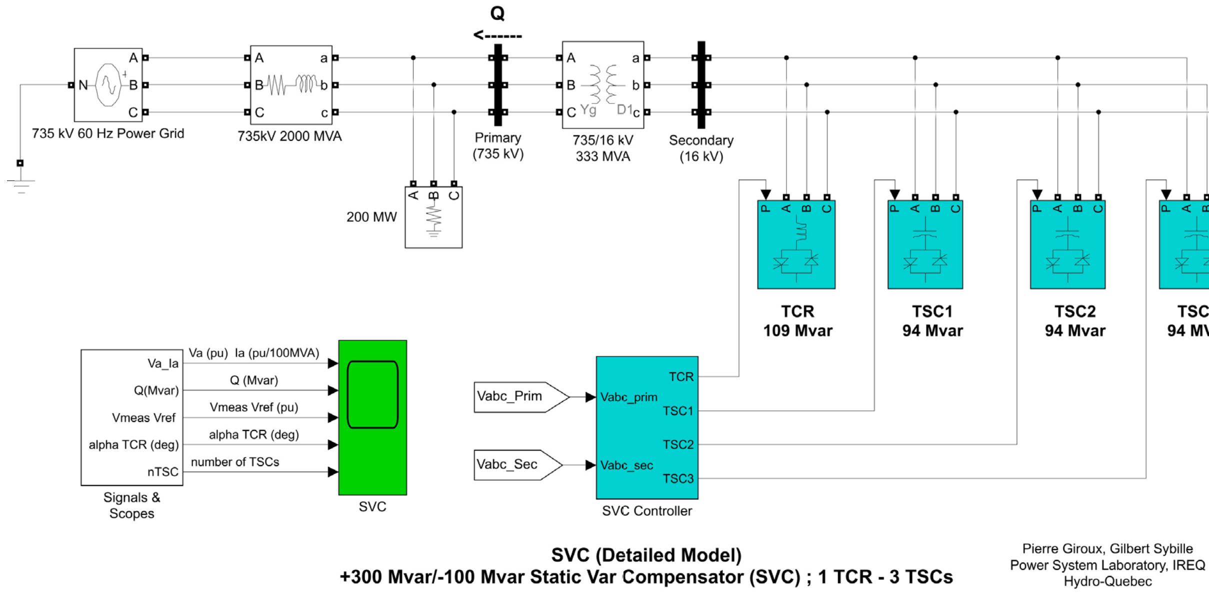

Fig. 1: Structure of the detailed SVC test bed in MATLAB/SimScape. Modified transmission line short-circuit power is 2000 MVA.

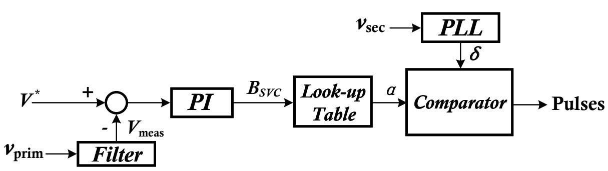

Fig. 2: SVC controller structure.

TABLE I: Parameters of the EMT testbed

Category	Description	Parameter	Value
System	Base Power	P_b	100 MVA
	Short-circuit Power	P_{sc}	2000 MVA
	Rated Voltage	V_n	735 kV, 16 kV
	Nominal Frequency	f_n	60 Hz
Passives	X/R ratio	X/R	10
	Line reactance	X_g	0.05 p.u.
	Line resistance	R_g	0.005 p.u.
	Load	P_{load}	200 MW
Controller	PLL-driven Filter	$k_{p,pll1}, k_{i,pll1}$	60, 1400
	Comparator PLL	$k_{k,pll2}, k_{i,pll2}$	120, 2800
	Voltage Regulator	k_p, k_i	10, 200
	Average Switching Delay	T_d	2.5 ms

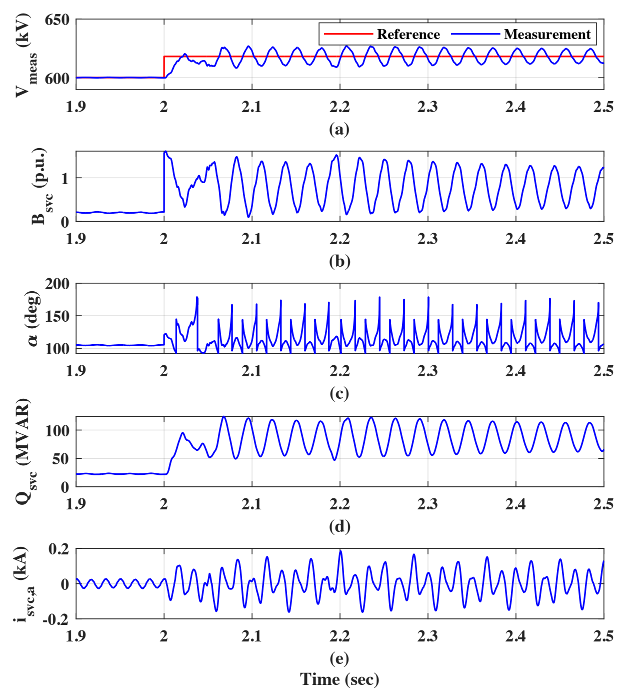

Fig. 3: Voltage reference increases by 0.03 p.u. Controller gains set to $k_p = 45$ and $k_i = 900$. (a) Voltage magnitude measurement; (b) Susceptance; (c) Firing angle; (d) Reactive power output of the SVC; (c) Phase A current flows from the SVC.

B. Critical Factors

In order to understand the potential causes of the oscillation and tackle this problem, time-domain experiments are done within the EMT simulation. The following critical factors and their influences are presented and compared.

1) Control parameters: At 2 seconds, the voltage regulator gains are set to be 6.4 times of the base values: $k_p = 64$, $k_i = 1280$. At 3 seconds, both the proportional and integral gains are set to be 6.5 times of the base values: $k_p = 65$ and $k_i = 1300$. The simulation results are shown in Fig. 5. According to the measurements, undamped oscillation appears and stays after the gains are increased. Therefore, it can be seen that increasing the voltage regulator's control parameters can cause oscillations.

2) Grid strength: On the network side, the grid strength is also important. To investigate the impact of grid strength, the line impedance (X_g) is increased to 1.5 times and twice of its base value respectively for the same control parameters: $k_p =$

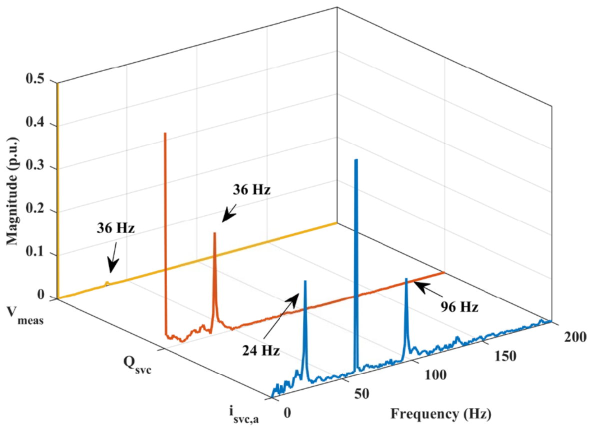

Fig. 4: Spectrum of V_{meas}, Q_{svc}, $i_{svc,a}$.

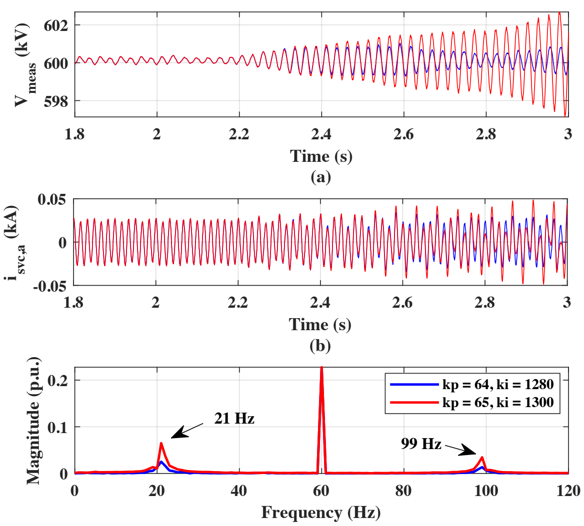

Fig. 5: At 2 seconds, control parameters increase. Blue lines indicate $k_p = 64$ and $k_i = 1280$. Red lines indicate $k_p = 65$ and $k_i = 1300$. (a) Voltage magnitude measurement (V_{meas}); (b) Phase A current from SVC ($i_{\text{svc,a}}$); (c) Spectrum of $i_{\text{svc,a}}$.

25 and $k_i = 500$. The simulation results of voltage magnitude (V_{meas}) are compared and presented in Fig. 6. Oscillations appear the grid impedance X_{g} increases. In addition, it can be clearly seen that the oscillation frequency also increases when X_{g} increases.

III. Measurement-based linear model extraction

In order to conduct further analysis to investigate the oscillation phenomenon, linear models of the system will be extracted from measurement data.

The feedback system structure is shown in Fig. 7, where the circuit model and firing unit are considered as one SISO model, $G(s)$. $G(s)$ will be estimated using the measurement data. The measurement test bed is built by disabling the voltage control of the SVC. The only control signal from the SVC is the fixed B_{SVC} command. A step response will be

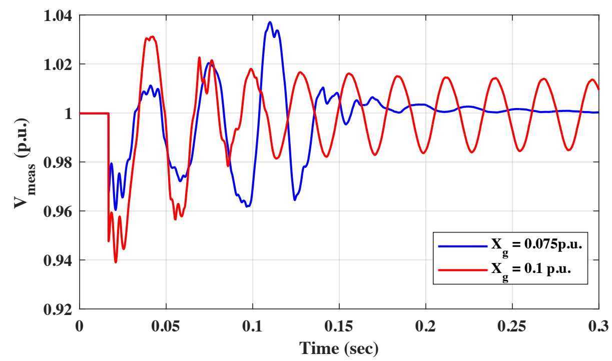

Fig. 6: Plot of V_{meas} when line impedance are 1.5 p.u. (blue) and 2 p.u. (red). Oscillation frequencies are around 28 and 36 Hz respectively.

injected into this command. The system's response, e.g., the POI voltage magnitude, will be recorded.

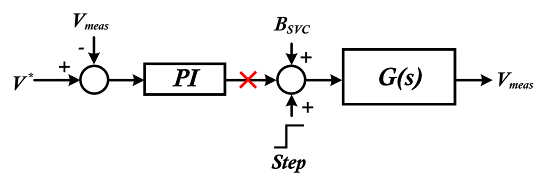

Fig. 7: Block diagram of measurement testbed topology.

A. Time-domain data

At steady-state, a step change with 0.1 p.u. magnitude is given on B_{SVC} after the PI controller is disconnected. The measurement of the filtered voltage magnitude from the EMT simulation is taken as the output signal. Fig. 8 presents the measurement data of the susceptance command B_{SVC} and the POI voltage V_{meas} at different line impedance levels. It can be seen that the ΔV's steady-state change is proportional to X_g, approximately.

B. Estimation

The System Identification Toolbox's `tfest` function is applied to estimate the input and output model $G(s)$ when $X_g = 0.05$ p.u. The estimation results are compared with the measurement data in Fig. 9, and the degree of matching is 94.95% and indicates the accuracy of the estimated model.

In Fig. 8, the measurement data from the simulation due to the step change appear as a typical second-order system with delay. After a few attempts, it is found that the estimation provides better fitting result when the IO delay is considered, which also allows a lower order for the estimation. The final setup is a second-order linear model with 2 poles, 1 zero, and an 0.0025 seconds of IO delay, and estimated model is shown as follows.

$$G(s) = \mathbf{exp}(-0.0025s)\frac{-1.256s + 1198}{s^2 + 262.3s + 2.502e04}. \quad (1)$$

Remarks: The obtained model is a second-order system with delay for $G(s) = \frac{V_{\text{meas}}}{B_{\text{SVC}}}$. For the widely adopted CIGRE

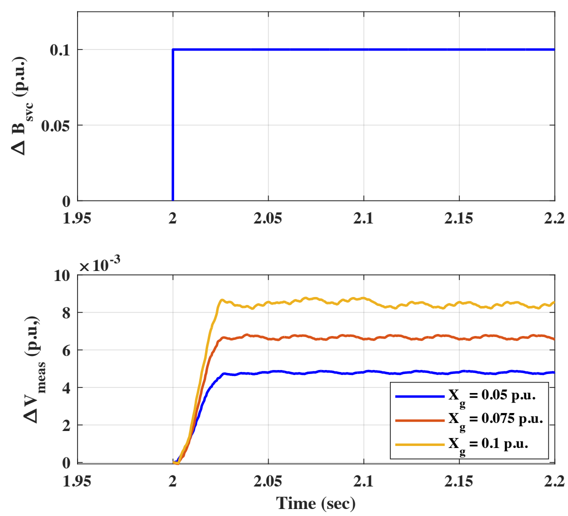

Fig. 8: Measurements corresponding to step change events at different X_{g}: (a) B_{SVC}; (b) V_{meas}.

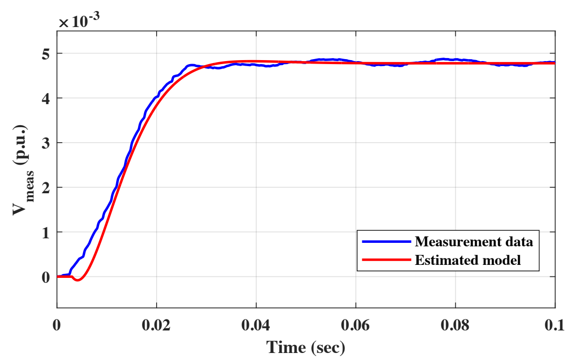

Fig. 9: Step responses matching among the EMT simulation measurement data and estimated model with 2 poles, 1 zero, and 0.0025 seconds of IO delay. $X_{\mathrm{g}} = 0.05$ p.u. 94.95% matching degree is achieved.

model for RMS-based dynamic simulation, the transfer function between the susceptance and the commend is as follows [11]:

$$B_{\mathrm{SVC}} = \frac{e^{-T_d s}}{1 + Ts} B^*_{\mathrm{SVC}} \tag{2}$$

where T_d is related to digital control delay and is assumed to be 1 ms. T includes thyristor firing delay and is in the range of 3 ms to 6 ms.

If this model is adopted, it can be seen $G(s)$ is also in the format of a first-order system with a delay. Apparently, from measurement-based estimation, a second-order system with a delay can better capture the dynamics. In our future research, why the second-order system with a delay can provide a better representation will be further investigated using analytical derivation approach.

IV. Stability Analysis

Three sets of methods (the root-locus method, the Bode plots, and the closed-loop eigenvalue analysis) are performed to provide stability analysis.

A. The Root-Locus Method

As the voltage control dynamic is not included in the measurement test bed, $G(s)$ obtained from estimation does not include the control dynamics (expressed as $C(s) = 10+200/s$). Therefore, Root-locus analysis is performed on the open-loop system $OL(s)$ after adding back the control dynamics:

$$OL(s) = G(s) \cdot C(s).$$

The root-locus method can easily examine the impact the controller gain on stability. Note that MATLAB's `rlocus` command does not work with model includes IO delay. Thus, the IO delay was manually removed and added back using the Pade approximation expression $T_d(s) = \frac{1-\tau_d/2s}{1+\tau_d/2s}$, where τ_d is the 0.0025 seconds delay time.

Fig. 10 presents the root-locus analysis plot, where the blue trajectory indicates original firing delay time constant is used ($\tau_d = 0.0025$ s) , and the red trajectory reflects the root loci when $\tau_d = 0.005$ s.

The marginal gain of the blue line is 6.6, indicating the system is unstable if the voltage control gains are increased to 6.6 times of the base value. In addition, the oscillating frequency is 42.1 Hz. This analysis results agree with the EMT simulation results shown in Fig. 5: when the gains are 6.5 times of the original values, 40 Hz oscillations appear in voltage RMS. Moreover, the root loci show that a larger time delay lowers the stability margin and the oscillation frequency.

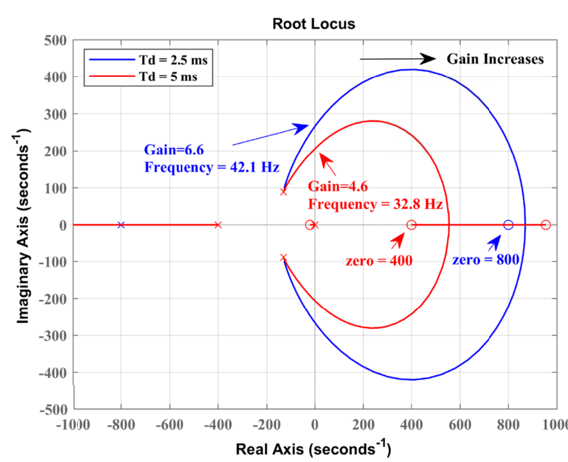

Fig. 10: Root locus plot of the system with various delay.

Remarks: It can be seen clearly in the root loci plots that the system has open-loop zeros located in the RHP. The one close to the imaginary axis is introduced by the delay and attracts a pair of complex conjugate eigenvalues (the oscillation mode) moving toward the RHP. Increasing the delay makes the RHP zero more close to the original point and provides more attracting force to the oscillation modes.

B. Bode plots

Sensitivity analysis can also be performed via frequency responses comparison. In Fig. 11, the open-loop system ($G(s)$) frequency-responses for $X_g = 0.05$ p.u. and $X_g = 0.1$ p.u. are plotted together with the inverse of the PI controller ($1/C(s)$). Two sets gains are (2.5 and 6.5 times of the base values) are examined.

It can be seen that increasing the line impedance or increasing the controller gain all lead to larger cross-over frequencies with larger phase difference, indicating worse stability. The analysis results corroborate with the EMT simulation results in Fig. 5 and Fig. 6.

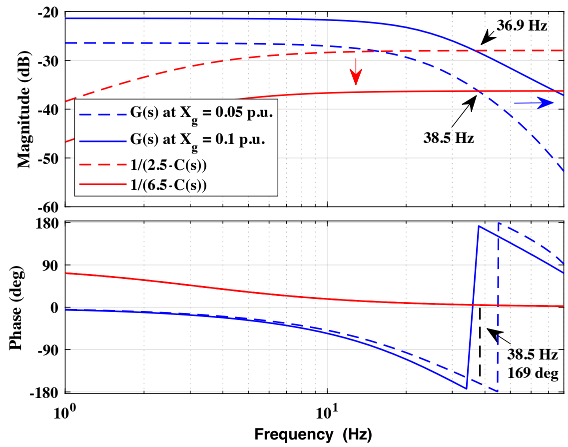

Fig. 11: Bode plots for sensitivity analysis against control parameters and grid impedance.

C. Eigenvalue-loci analysis

In addition to the stability analysis conducted to identify the impact of major aspects, the following eigenvalue-based analysis based on the closed-loop system ($CL(s)$) reveals the influence on stability due to the proportional gain and integral gain respectively. Based on the estimated linear model $G(s)$, the controller transfer function $C(s)$, the closed-loop system is as follows: $CL(s) = \frac{C(s)G(s)}{1+C(s)G(s)}$.

By increasing the proportional and integral gain individually, the system eigenvalues move to the RHP gradually as shown in Fig. 12. From comparison, it presents that system becomes unstable when proportional gain is increased by 7 times, while the increasing the integral gain by 10 times does not cause instability. Also, the unstable marginal oscillation frequency is observed to be affected by the value of the proportional gain. It is indicated that the proportional gain tuning is more sensitive and critical than the integral gain, which agrees with the observations from other literature [6], [7].

V. Conclusion

The sub-synchronous oscillation phenomenon in SVCs is investigated and presented in this paper. Based on the linear model extracted from the measurement data, it can be concluded that the root causes of oscillations are mainly due to

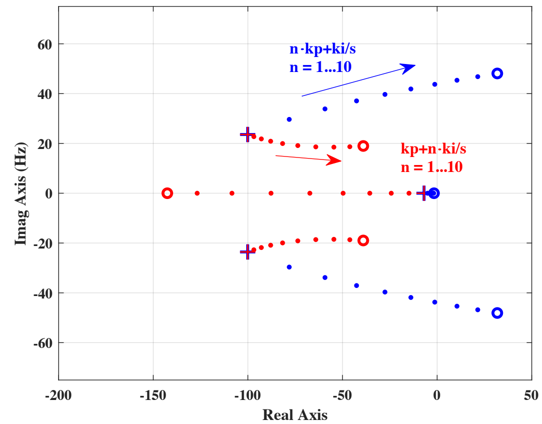

Fig. 12: Eigenvalue-loci plot of the closed-loop system to compare impacts of proportional gain and integral gain. Base case: $k_p = 1$ and $k_i = 50$. For the gain increasing case, the k step leads to a gain of $(0.5k+1)k_p$ or $(0.5k+1)k_i$.

the thyristor firing unit delay at a scale of 2.5 ms. This delay contributes a zero in the RHP. Increasing the voltage control gain will make a pair of eigenvalues move toward the RHP. A reducing grid strength also contributes to instability.

References

[1] E. V. Larsen, N. W. Miller, S. L. Nilsson, and S. R. Lindgren, "Benefits of gto-based compensation systems for electric utility applications," *IEEE Transactions on power delivery*, vol. 7, no. 4, pp. 2056–2064, 1992.

[2] R. Gutman, J. J. Keane, M. E. Rahman, and O. Veraas, "Application and operation of a static var system on a power system american electric power experience, part i: System studies experience, system," *IEEE Power Engineering Review*, vol. PER-5, no. 7, pp. 55–56, 1985.

[3] ——, "Application and operation of a static var system on a power system americal electric power experience part ii: Equipment design and installation," *IEEE Transactions on Power Apparatus and Systems*, vol. PAS-104, no. 7, pp. 1875–1881, 1985.

[4] D. Dickmander, B. Thorvaldsson, G. Stromberg, D. Osborn, A. Poitras, and D. Fisher, "Control system design and performance verification for the chester, maine static var compensator," *IEEE Transactions on Power Delivery*, vol. 7, no. 3, pp. 1492–1503, 1992.

[5] L. Gerin-Lajoie, G. Scott, S. Breault, E. Larsen, D. Baker, and A. Imece, "Hydro-quebec multiple svc application control stability study," *IEEE transactions on power delivery*, vol. 5, no. 3, pp. 1543–1551, 1990.

[6] M. Parniani and M. Iravani, "Voltage control stability and dynamic interaction phenomena of static var compensators," *IEEE transactions on power systems*, vol. 10, no. 3, pp. 1592–1597, 1995.

[7] H. Shi, X. Sun, G. Chen, H. Zhang, Y. Tang, L. Xu, L. Ding, C. Fan, and Y. Xu, "Optimization strategy of svc for eliminating electromagnetic oscillation in weak networking power systems," *Energies*, vol. 12, no. 18, p. 3489, 2019.

[8] X. Sun, B. Zhou, P. Liu, X. Xie, J. Shair, X. Chang, and W. Wei, "Investigating sub-and super-synchronous interaction between static var compensators and a weak ac grid," in *The 16th IET International Conference on AC and DC Power Transmission (ACDC 2020)*, vol. 2020. IET, 2020, pp. 639–644.

[9] D. Jovcic, N. Pahalawaththa, M. Zavahir, and H. A. Hassan, "Svc dynamic analytical model," *IEEE transactions on power delivery*, vol. 18, no. 4, pp. 1455–1461, 2003.

[10] P. Giroux and G. Sybille, "Svc detailed model." [Online]. Available: https://www.mathworks.com/help/physmod/sps/ug/svc-detailed-model.html;jsessionid=baac159418f9a53a02b167158dff

[11] "Static var compensator models for power flow and dynamic performance simulation," *IEEE Transactions on Power Systems*, vol. 9, no. 1, pp. 229–240, 1994.